2010 IEEE International Conference on Robotics and Automation
Anchorage Convention District
May 3-8, 2010, Anchorage, Alaska, USA

A Compact Rotary Series Elastic Actuator for Knee Joint Assistive System

Kyoungchul Kong, *Member, IEEE*, Joonbum Bae, *Student Member, IEEE*,
Masayoshi Tomizuka, *Fellow, IEEE*

***Abstract*—Precise and large torque generation, back-drivability, low output impedance, and compactness of hardware are important requirements for human assistive robots. In this paper, a compact rotary series elastic actuator (cRSEA) is designed considering these requirements. To magnify the torque generated by an electric motor in the limited space of the compact device, a worm gear is utilized. However, the actual torque amplification ratio provided by the worm gear is different from the nominal speed reduction ratio due to friction, which makes the controller design challenging. In this paper, the friction effect is considered in the model of cRSEA, and a robust control algorithm is designed to precisely control the torque output in the presence of nonlinearities such as the friction. The mechanical design and dynamic model of the proposed device and the design of a robust control algorithm are discussed, and actuation performance is verified by experiments.**

I. Introduction

HUMAN assistive robots, i.e., systems that assist human motions with actuation capabilities, have been intensively developed in recent years based on mechatronic and robotic technologies [1-5]. To effectively assist human motions, such systems are required to generate large torques (e.g., over 30Nm is required to fully support the knee joint during normal walking). While generating such large torques, high precision is also required for natural assistance. Moreover, the assistive robots should be compact and light to minimize discomforts caused by the robot hardware, which imposes a constraint on the selection of actuators. To fulfill these requirements, electric motors equipped with gear reducers have been often utilized in the human assistive robots. However, not only do the gear reducers amplify the motor torque by reducing the rotor speed, but they also increase the mechanical impedance of the system significantly. In addition, the gear reducers decrease compliance of the actuator, which is not desirable from the viewpoint of safety. Moreover, nonlinearities inherent in the gear reducers (e.g., friction and backlash) make the precise torque control challenging.

To overcome such drawbacks of the geared motors while taking advantage of their superior controllability and high power-mass density, series elastic actuators have been devised [1-5]. The series elastic actuators are actuator modules that consist of an electric motor and a spring. The spring placed between the actuator and the human joint plays the role of a torque sensor as well as an energy buffer, which allows the precise control of generated torque. Since the spring is able to immediately store the impact forces exerted from the human joint, compliance can also be easily guaranteed depending on the control algorithm.

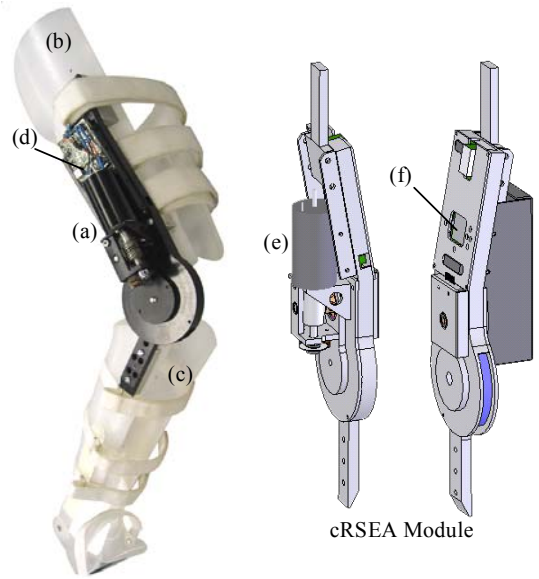

Fig. 1. Compact series elastic actuator designed for assisting the knee joint. It consists of (a) the proposed cRSEA module, (b) a thigh brace, (c) a calf brace, (d) a motor driver, (e) a DC motor, and (f) an embedded controller.

In our previous work, a rotary series elastic actuator (RSEA) and its robust control algorithm were presented [9]. The RSEA utilizes a torsion spring and a geared DC motor. A disturbance observer was applied to precisely control the RSEA in the presence of nonlinearities inherent in the geared motor and model uncertainties caused by human-robot interactions. The proposed methods have shown good performance in practice (i.e., back-drivability, low impedance, precise torque control, etc) and have applied to actual assistive robots.

In this paper, an improved design of the RSEA, a compact rotary series elastic actuator (cRSEA), and its control algorithm are proposed. The cRSEA is designed for knee joint assistance, and thus the design parameters are optimized to assist knee joint motions. In the previous RSEA, a spring

Manuscript received September 15, 2009. This work was supported in part by the National Science Foundation under Grant CMMI 0800501.

The authors are with the Department of Mechanical Engineering, University of California, Berkeley, CA 94720 USA (e-mail: {kckong, jbbae, tomizuka}@me.berkeley.edu).

was directly installed between the shaft of the geared motor and the human joint, a consequence of which was a very stiff spring in order to generate large assistive torques. However, the stiff spring deteriorates compliance of the system and makes the precise torque control difficult. Also, nonlinearities of the spring, such as a nonlinear spring constant, are not negligible in case of the stiff springs. In the cRSEA proposed in this paper, a spring is installed in the chain of gears, so that an optimal spring can be utilized. The use of a small spring also contributes to the compact design of the system.

In the cRSEA, a worm gear is used as well as spur gears to amplify the torque generated by an electric motor. However, the torque amplification ratio of the worm gear is sensitive to the friction coefficient, which introduces an uncertainty to the system model. Therefore, the dynamic model of cRSEA is obtained considering the friction between the worm gear and the worm wheel. Since the cRSEA is exposed to large model variations as well as disturbances due to interactions with humans, a robust control method is required. In this paper, a control algorithm inspired by the disturbance observer is proposed. The controller design procedure is discussed based on experimental data, in particular, frequency responses of the system.

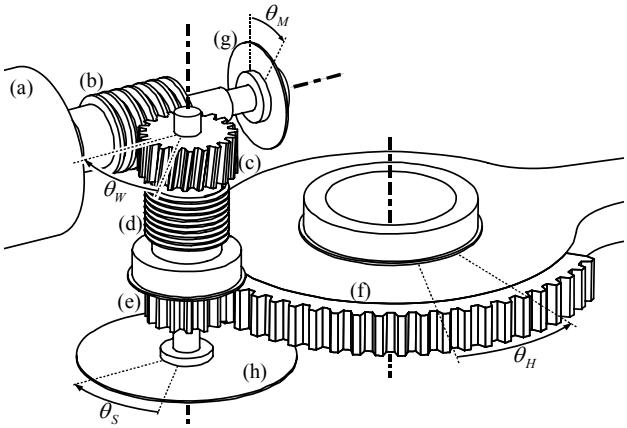

Fig. 2. Power transmission mechanism of cRSEA. (a) Maxon RE40 DC motor, (b) a worm gear, (c) a worm wheel, (d) a torsional spring, (e) a small spur gear (fifteen teeth), (f) a knee frame with a large spur gear (ninety teeth), (g) an encoder on the motor side, and (h) an encoder on the human side.

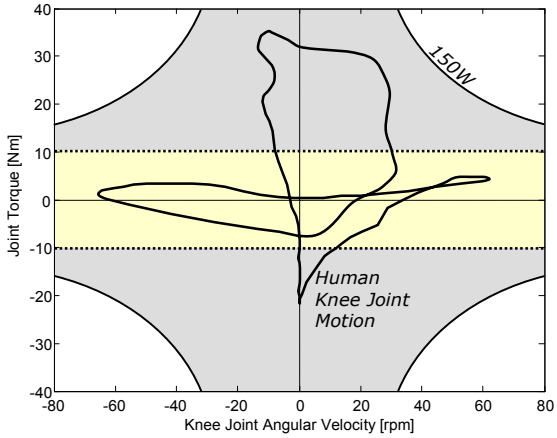

Fig. 3. The range of knee joint motions during normal walking. The range that a 150W DC motor can support is also shown in the figure.

II. Mechanical Design of Compact Rotary Series Elastic Actuator

The compact rotary series elastic actuator (cRSEA) consists of 1) a DC motor, 2) a worm gear set, 3) a spur gear set, 4) a torsion spring, 5) two high resolution encoders, 6) a motor driver, and 7) an embedded micro controller (Luminary Stellaris LM3S8962 board [10]), as shown in Figs. 1 and 2. In this section, the mechanical design and the dynamic model of the cRSEA are introduced.

A. Selection of a DC Motor and Gears

In order to assist human motions with sufficiently large assistive torques, an electric motor should be selected considering the characteristics of human motions. Note that the capacity of a motor is determined by the maximum power, and thus the maximum torque and angular velocity required to assist human motions are of important factors in the selection of a motor. The cRSEA proposed in this paper is designed for assisting a knee joint, and Fig. 3 shows the knee joint torque and angular velocity occurred in one stride of a normal gait. The data is obtained from a male subject with the body weight of 70 kg. The maximum power consumed by the knee joint is about 80 W. Considering the safety factor of two, a motor of 150 W, RE40 DC motor of Maxon Motor Company, is selected. The area surrounded by the continuous lines labeled by *150W* [i.e., the grey and yellow area in Fig. 3] represents the operation range of the selected motor.

In electric motor systems, the maximum speed and torque are limited. In case of the RE40 motor, the maximum continuous speed and torque are respectively 8200 rpm and 0.181 Nm, while the angular velocities of the knee joint during normal walking are in the range of $\pm$ 60 rpm, as shown in Fig. 3. Note that the operation range can be adjusted by utilizing a gear reducer. To guarantee the immediate responses to the knee joint motions, the desired range of the angular velocity of the knee frame [(f) in Fig. 2] is set to $\pm$ 120 rpm, which is twice faster than the knee joint motion. Based on these numbers, the speed reduction ratio is selected to 60:1, where 10:1 comes from the worm gear and the worm wheel [(b) and (c) in Fig. 2] and 6:1 comes from the spur gears [(e) and (f) in Fig. 2]. Note that the reduced maximum speed results in the increased maximum torque. If the efficiency of the gears is not considered, the torque generated by the motor is amplified by the speed reduction ratio, i.e., the cRSEA system may generate the assistive torques up to 10.87 Nm. However, friction between the worm gear and the worm wheel significantly lowers the efficiency, and the torque amplification ratio is not necessarily the same as the speed reduction ratio. The details on the torque amplification ratio will be discussed in Section II-*D*.

Note that the maximum torque for short duration is significantly larger than the maximum continuous torque. For example, the stall torque of the RE40 motor, i.e., the maximum torque that can be generated by the motor at zero speed, is 2.290 Nm, which is 1,200% larger than the

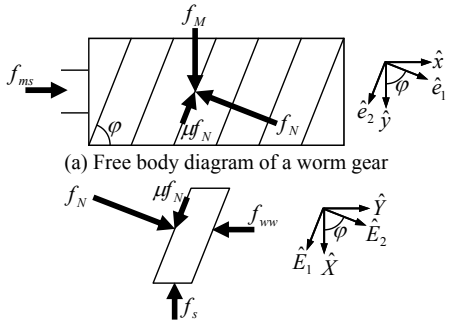

(a) Free body diagram of a worm gear

(b) Free body diagram of one tooth of the worm wheel

Fig. 4. Free body diagrams of the worm-gear and worm-wheel. f_M represents the force generated by the motor, and f_{ww}, f_{ms}, and f_s represent the reaction forces by the worm-wheel, the motor shaft, and the worm-wheel shaft, respectively.

maximum continuous torque. Therefore, the proposed cRSEA is capable of generating the assistive torques up to 130 Nm in the limited conditions. However, it is reasonable to assume that the motor is to generate the assistive torque continuously, and therefore the desired range of the assistive torque is regarded as $\pm$ 10 Nm, as shown in Fig. 3 [the yellow area between the dotted lines in the figure].

B. Kinematic Model

Fig. 2 shows the power transmission mechanism of the proposed cRSEA. The torque generated by the motor [(a) in the figure] is amplified by two sets of gears, the worm gear set [(b) and (c)] and the spur gear set [(e) and (f)]. The frame [(f) in the figure] is connected to the calf brace, while the main frame is fixed on the thigh brace. Therefore, θ_H represents the knee joint angle. The motor angle, θ_M, and the angle of the small spur gear, θ_S, are measured by high resolution encoders.

By a simple calculation, the knee joint angle, θ_H, can be obtained, i.e.

$$\theta_H = N_S^{-1}\theta_S \tag{1}$$

where N_S is the speed reduction ratio between the spur gears [(e) and (f) in Fig. 2]. In the actual design, $N_S = 6$.

Similarly, a pair of the worm gear and the worm wheel provides the speed reduction ratio of N_W. When the worm gear rotates one revolution, one pitch of the worm wheel is rotated. Therefore, the worm gear acts as a single toothed gear, and thus the gear ratio is the same as the number of teeth of the worm wheel. Since one revolution of the worm gear corresponds to one pitch of the worm wheel, the following kinematic condition is satisfied.

$$2\pi r_{wg}[\tan\varphi]^{-1} = 2\pi r_{ww}N_W^{-1} \tag{2}$$

where r_{wg} and r_{ww} are the radii of the worm gear and the worm wheel, respectively. φ is the distortion angle of the worm gear shown in Fig. 4. Note that (2) can be simplified to $N_W = [r_{ww}/r_{wg}]\tan\varphi$.

C. Dynamic Model

Fig. 4 shows the free body diagrams of the worm gear and worm wheel used in the cRSEA [i.e., (b) and (c) in Fig. 2]. The force vectors in Fig. 4 are acting on the point that the worm gear contacts the worm wheel. Note that the contact point moves only in the direction of $\hat{y}$ or $\hat{Y}$ due to mechanical constraints.

The force balance equations are

$$\frac{1}{r_{wg}}I_M\ddot{\theta}_M\hat{y} = f_M\hat{y} + f_{ms}\hat{x} - f_N\hat{e}_1 - \mu f_N\hat{e}_2 \tag{3}$$

$$\frac{1}{r_{ww}}I_{ww}\ddot{\theta}_W\hat{Y} = -f_{ww}\hat{Y} - f_s\hat{X} + f_N\hat{E}_2 + \mu f_N\hat{E}_1 \tag{4}$$

where f_M, f_{ww}, f_{ms}, and f_s are as defined in Fig. 4, and I_M and I_{ww} are the inertias of the motor and the worm wheel, respectively. I_M includes the inertia of the worm gear. r_{wg} and r_{ww} are the radii of the worm gear and the worm wheel, respectively. μ represents the friction coefficient between the worm gear and the worm wheel.

The dot product of (3) and $\hat{y}$ is

$$\frac{1}{r_{wg}}I_M\ddot{\theta}_M = f_M - f_N\cos\varphi - \mu f_N\sin\varphi \tag{5}$$

Similarly,

$$\frac{1}{r_{ww}}I_{ww}\ddot{\theta}_W = -f_{ww} + f_N\sin\varphi + \mu f_N\cos\varphi \tag{6}$$

The normal force, f_N, can be eliminated by rearranging (5) and (6), i.e.

$$f_{ww}r_{ww} + I_{ww}\ddot{\theta}_W = [f_M r_{wg} - I_M\ddot{\theta}_M]\frac{r_{ww}(\sin\varphi + \mu\cos\varphi)}{r_{wg}(\cos\varphi + \mu\sin\varphi)} \tag{7}$$

Note that $f_{ww}r_{ww} = \tau_{ww}$ and $f_M r_{wg} = \tau_M$, where τ_{ww} is the torque applied to the worm wheel and τ_M is the torque generated by the motor. τ_{ww} includes the torque by a spring deflection, $k(\theta_W - \theta_S)$, as well as the torque exerted from the human side, τ_H, i.e.

$$\tau_{ww} = k(\theta_W - \theta_S) + N_S^{-1}\tau_H \tag{8}$$

where k is the spring constant, and N_S is the speed reduction ratio of the spur gears. In (8), the friction between the spur gear set is neglected. Since θ_M and θ_W are related by the gear ratio of the worm gear set [i.e., $\theta_M = N_W\theta_W$], (7) can be rewritten as

$$N_S k(\theta_W - \theta_S) = N_S A(\varphi,\mu)\left[\tau_M - \left(\frac{I_{ww}}{N_W A(\varphi,\mu)} + I_M\right)\ddot{\theta}_M\right] - \tau_H \tag{9}$$

where

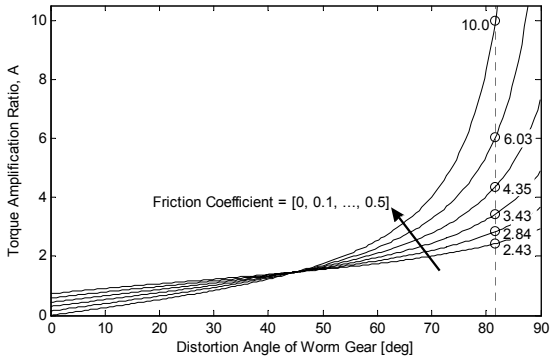

Fig. 5. Torque amplification ratio. The nominal value (i.e., when the friction is neglected) is 10.0, which is the same as the speed reduction ratio.

$$A(\varphi,\mu)=\frac{r_{ww}(\sin\varphi+\mu\cos\varphi)}{r_{wg}(\cos\varphi+\mu\sin\varphi)} \tag{10}$$

$A(\varphi, \mu)$ in (10) is a torque amplification ratio of the worm gear and the worm wheel. In the actual cRSEA, the distortion angle of the worm gear, φ, is fixed, but the friction coefficient, μ, may vary depending on the lubricant or temperature conditions. Note that the torque amplification ratio is the same as the speed reduction ratio, when the friction coefficient is zero, i.e., $A(\varphi, 0) = N_W = [r_{ww}/r_{wg}]\tan\varphi$. However, in the presence of friction, a power loss occurs and the torque is not amplified as desired. Fig. 5 shows the magnitude of $A(\varphi, \mu)$ for some selected friction coefficients and gear angles. The dotted line in the figure represents the gear angle used in the actual design of cRSEA. Note that when $\mu = 0$, the torque amplification ratio is 10.0, which is the speed reduction ratio, N_W. In Fig. 5, it should be noted that the torque amplification ratio changes drastically according to the variation of the friction coefficient. The variation in the torque amplification ratio shown in Fig. 5 introduces model uncertainties to the system.

The dynamic model in (9) implies that the cRSEA is a multi-input and multi-output system, where the inputs are the motor torque [τ_M, control input] and the human joint torque [τ_H, disturbance input], and the outputs are the motor angle [θ_M] and the angle of the spur gear [θ_S]. The generated torque can be calculated by Hooke's law from the measured angles.

III. Controller Design of Compact Rotary Series Elastic Actuator

The performance objectives of the cRSEA are 1) to precisely generate the desired torque in the presence of model uncertainties and external disturbances, 2) to minimize the mechanical impedance, and 3) to minimize the influence of human motions in the generated torques. In (9), note that the torque output, $\tau_O = N_S k(\theta_W - \theta_S)$, is influenced by the torques exerted from the human side, τ_H, and the angular acceleration of the motor shaft, $\ddot{\theta}_M$. The variation in $A(\varphi, \mu)$ also introduces an uncertainty to the system. In this section, a robust control algorithm is designed to achieve the performance objectives considering these factors.

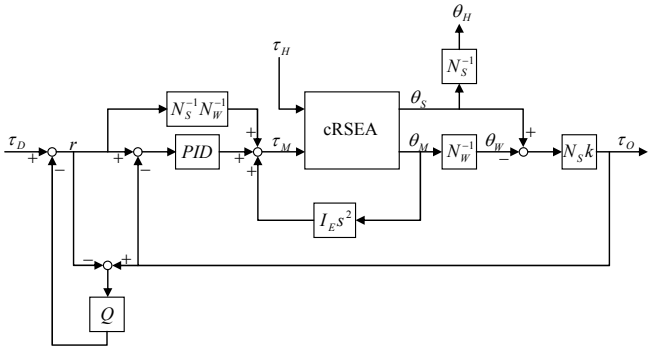

Fig. 6. Block diagram of the proposed control law. The notations represent: N_W: the speed reduction ratio of the worm gear set, N_S: the speed reduction ratio of the spur gear set, *PID*: the PID controller in (11), I_E: the extended motor inertia to compensate for the motor dynamics.

A. Controller Design

Suppose the following control law:

$$\begin{aligned}\tau_M &= I_E\ddot{\theta}_M + N_S^{-1}N_W^{-1}r \\ &\quad + K_P(r-\tau_O) + K_D(\dot{r}-\dot{\tau}_O) + \int(r-\tau_O)dt\end{aligned} \tag{11}$$

where $I_E = I_{ww}/N_W^2 + I_M$, which is the extended motor inertia. r is the reference input, and τ_O is the torque output generated by the spring [i.e., $\tau_O = N_S k(\theta_W - \theta_S)$]. Note that τ_O can be directly calculated from $\theta_W = N_W^{-1}\theta_M$ and θ_S, which are measured by encoders. The parameters K_P, K_D, and K_I are controller gains to have the torque output follow the reference input. Note that the proposed control law consists of three parts: 1) the extended motor dynamics [i.e., $I_E\ddot{\theta}_M$] that compensates for the motor inertia, 2) the feedforward input [i.e., $N_S^{-1}N_W^{-1}r$], and 3) the PID controller. Fig. 6 shows the block diagram of the proposed control law.

For simplicity, suppose that the motor dynamics is cancelled by the extended inertia included in (11). By applying the Laplace transformation to the remaining closed loop dynamics, a transfer function is

$$\tau_O = G_{R\to O}(s)r - G_{H\to O}(s)\tau_H \tag{12}$$

where

$$G_{R\to O}(s)=\frac{K_D s^2+(K_P+N_S^{-1}N_W^{-1})s+K_I}{K_D s^2+(K_P+N_S^{-1}A^{-1})s+K_I} \tag{13}$$

$$G_{H\to O}(s)=\frac{N_S^{-1}A^{-1}s}{K_D s^2+(K_P+N_S^{-1}A^{-1})s+K_I} \tag{14}$$

where τ_D is the desired assistive torque output, and $G_{R\to O}(s)$ and $G_{H\to O}(s)$ are the transfer functions to the torque output from the reference input and the human joint torque, respectively.

The controller gains K_P, K_D, and K_I can be designed considering the desired closed loop poles. In the controller design, the torque amplification ratio, $A(\varphi, \mu)$, is regarded as its nominal value, N_W. For example, if the desired closed loop poles are $-p_1$ and $-p_2$, the controller gains are obtained by $(K_P + N_S^{-1}N_W^{-1})/K_D = p_1 + p_2$ and $K_I/K_D = p_1p_2$. Note that $G_{H\to O}(s)$ and $G_{H\to O}(s)$ respectively become close to 1 and 0, as the magnitude of controller gains increases. However, the high gain control causes discomfort due to chattering in the torque output, which is not desirable in practice.

Suppose that the reference input, r, is determined based on the desired torque, τ_D, and the difference between the generated torque and the reference input, $\tau_O - r$, i.e.

$$r = \tau_D - Q(s)[\tau_O - r] \tag{15}$$

where $Q(s)$ is a filter that smoothens the torque error, which plays the role similar to the Q filter in disturbance observers [5], [6]. Rearranging (15), $r = [1-Q(s)]^{-1}\tau_D - Q(s)[1-Q(s)]^{-1}\tau_O$, which implies that the torque output is fed back into the system via the reference input as well as the control input.

Substituting (15) into (12),

$$\tau_O = G^*_{D\to O}(s)\tau_D - G^*_{H\to O}(s)\tau_H \tag{16}$$

where

$$G^*_{D\to O}(s)=\frac{G_{R\to O}(s)}{1-Q(s)+G_{R\to O}(s)Q(s)} \tag{17}$$

$$G^*_{H\to O}(s)=\frac{[1-Q(s)]G_{H\to O}(s)}{[1-Q(s)+G_{R\to O}(s)Q(s)]AN_S} \tag{18}$$

The actuator is required to precisely generate the desired torque regardless of the human joint torques or motions. Therefore, the desired transfer function is $\tau_O = \tau_D$, which requires $G^*_{D\to O}(s) = 1$ and $G^*_{H\to O}(s) = 0$. Note that if $Q(s) = 1$, such conditions are satisfied. Therefore, $Q(s)$ should be designed such that $Q(j\omega) = 1 + 0j$ at frequencies where the precise torque generation is required.

B. Robust Stability

The characteristic equation of the transfer function in (16) is $1 - Q(s) + G_{R\to O}(s)Q(s) = 0$. Note that $G_{R\to O}(s)$ is subject to change due to the variations in $A(\varphi, \mu)$, which is resulted from the variation in the friction coefficient. Moreover, I_E in (11) also includes N_W, the nominal value of $A(\varphi, \mu)$. To encounter such uncertainties, multiplicative uncertainties imposed on the system model are considered, i.e.

$$G_{R\to O}(s)=1+W(s)\Delta(s) \tag{19}$$

where $W(s)$ is a stable boundary function of the multiplicative uncertainties, and $\Delta(s)$ is a random but stable transfer function with bounded magnitude, i.e., $\|\Delta\|_\infty < 1$. Note that in (19), the nominal model of $G_{R\to O}(s)$ is $1(s)$, because $G_{R\to O}(s) = 1$ when $A(\varphi, \mu) = N_W$ [see Eq. (13)].

Substituting (19) into the characteristic equation of (16),

$$1+W(s)\Delta(s)Q(s)=0 \tag{20}$$

Eq. (20) introduces a constraint to the design of $Q(s)$. Note that $W(s)\Delta(s)Q(s)$ is stable by definition. Therefore, the system is stable unless $W(s)\Delta(s)Q(s)$ encircles $-1 + 0j$ on the Nyquist plot. However, $\Delta(s)$ is unknown, and thus it is difficult to directly apply the Nyquist method. A conservative way to guarantee the stability of the system is to apply the small gain theorem. Namely, the system is stable if (but not only if) $|W(j\omega)\Delta(j\omega)Q(j\omega)| < 1$ for all frequencies. Also, this condition is satisfied if

$$|Q(j\omega)|<|W(j\omega)|^{-1} \text{ for all } \omega\in\Re \tag{21}$$

Note that (20)–(21) follows the same principles of the disturbance observer design [9], [11].

IV. Implementation and Experiments

A. Selection of PID Gains

The PID gains in the control law (i.e., K_P, K_D, and K_I in system. Since the cRSEA is utilized to a knee assistive device (11)) are selected considering the desired bandwidth of the in this paper, it is reasonable to select the PID gains such that the closed loop bandwidth is larger than the natural frequency of the calf, which is about 5 rad/sec. In experiments, the PID gains are selected to $K_P = 5$, $K_D = 0.251$, and $K_I = 25.1$, which are resulted from $p_1 = p_2 = 10$.

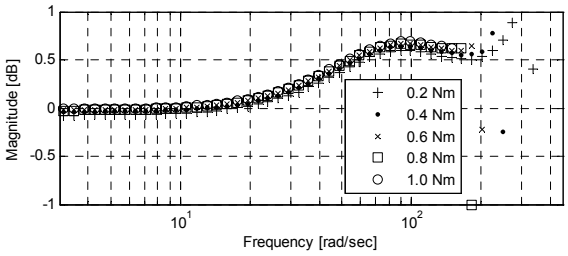

Fig. 7. Frequency responses of the PID-controlled cRSEA. The amplitudes of the excitation inputs (i.e., the desired torques) were varied from 0.2 Nm to 1.0 Nm.

Fig. 7 shows the frequency responses of the closed loop systems with various excitation amplitudes, where the input and the output are the desired and generated torques, respectively. In the experiments, the knee frame was mechanically fixed, and thus the responses in Fig. 7 may include the effect of external disturbances. Although the responses are close to 0 dB at low frequencies, they are apart from 0 dB at high frequencies. Also, the frequency responses are slightly changed for different excitation amplitudes, which implies the existence of nonlinearity in the system. Note that the responses are scattered at frequencies higher than 180 rad/sec, which is caused by the motor saturation. Although the saturation problem can be solved by decreasing the PID gains, the same gains are used in experiments because the frequency bandwidth of human motions is significantly lower than 180 rad/sec.

B. Design of Q Filter

In the proposed control law, the reference input, r, is determined by the torque error as well as the desired torque. In this procedure, a filter, $Q(s)$, is utilized as in (15). In the design of $Q(s)$, the following conditions should be fulfilled to guarantee robust stability; 1) $Q(s)$ must be stable, and 2) the magnitude of $Q(j\omega)$ should be less than that of $W^{-1}(j\omega)$ for all ω, where $W(s)$ is a boundary function of the multiplicative uncertainties.

Since the frequency responses from the reference input to the torque output have been obtained by experiments [see Fig. 7], the multiplicative uncertainties can be estimated by $W(j\omega)\Delta(j\omega) = G_{R\to O}(j\omega) - 1$. Fig. 8(a) shows the magnitude of the multiplicative uncertainties calculated from the results in Fig. 7. Based on the experimentally obtained information, $Q(s)$ can be designed to satisfy the robust stability condition. A possible $Q(s)$ is

$$Q(s)=\frac{2500}{s^2+70.5s+2500} \tag{22}$$

Note that $Q(s)$ in (22) has the cut-off frequency of 50 rad/sec and the magnitude of one at low frequencies. Also, it has the robust stability margin of at least 15 dB for all frequencies, as shown in Fig. 8(b).

The magnitude of $G^*_{H\to O}(j\omega)$ in (18) represents how much the torque output is affected by the human motions or human joint torques at the frequency ω. When the desired torque is zero, i.e., $\tau_D = 0$, the magnitude of $G^*_{H\to O}(j\omega)$ shows how large

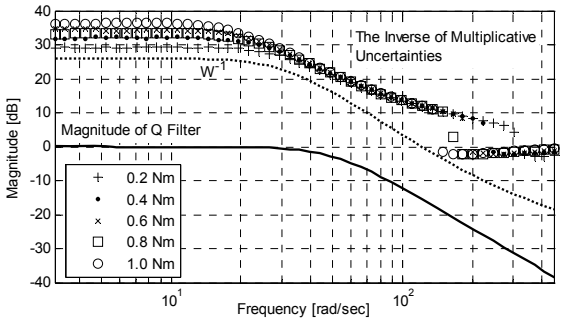

(a) Multiplicative uncertainties and a selected $Q(s)$

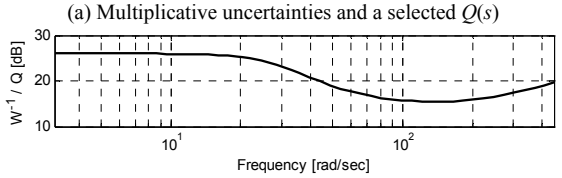

(b) Stability robustness margin, $W^{-1}(s) / Q(s)$

Fig. 8. Design of Q filter.

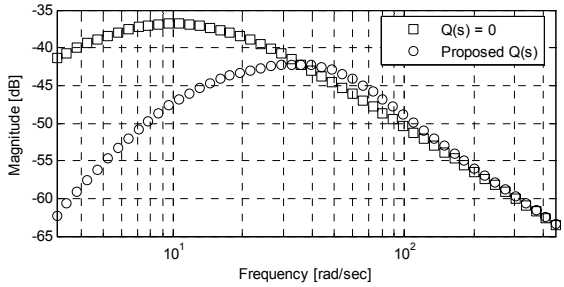

Fig. 9. Closed loop frequency responses from the human joint torque to the generated (resistive) torque with $Q(s)$ in (22) and $Q(s) = 0$.

resistive torque is generated to the human motions. Therefore, the magnitude of $G^*_{H\to O}(j\omega)$ is related to the mechanical impedance of the system, and is required to be minimized. Fig. 10 shows the magnitude of $G^*_{H\to O}(j\omega)$ with $Q(s)$ in (22) and $Q(s) = 0$. Notice that with the proposed $Q(s)$, the magnitude of $G^*_{H\to O}(j\omega)$ is significantly decreased up to 30 rad/sec, which is higher than the natural frequency of the calf.

Fig. 10 shows the frequency responses from the desired torque to the generated torque, i.e., $G^*_{D\to O}(j\omega)$. As discussed before, it is desired that $G^*_{D\to O}(j\omega) = 1 + 0j$ at frequencies where the precise torque generation is required. Note that the magnitude of $G^*_{D\to O}(j\omega)$ is close to one (0 dB) when the proposed $Q(s)$ is applied in the control law. Also, the phase of $G^*_{D\to O}(j\omega)$ is close to zero, which implies that the cRSEA immediately generates the desired torque without a phase delay.

The results in Figs. 9 and 10 confirm that the cRSEA controlled by the proposed control law can precisely generate the desired torque with the minimal influence of human joint torques or motions.

V. Conclusion

An actuator module for human assistive devices was proposed in this paper. The proposed device, a compact series elastic actuator, utilizes a torsion spring in the chain of spur gears and worm gears, which allows the precise control of the

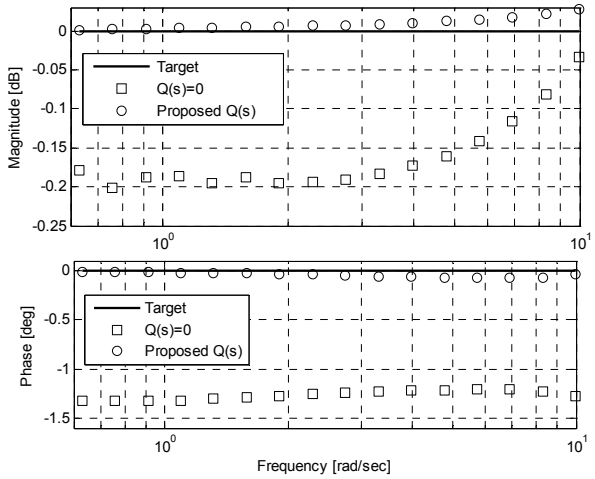

Fig. 10. Closed loop frequency responses from the desired torque to the generated torque with $Q(s)$ in (22) and $Q(s) = 0$.

generated assistive torque. A robust control algorithm inspired by disturbance observers was designed to control the proposed device. The performance of the proposed device and control algorithm (e.g., the minimal impedance and the precision of torque output) was verified by experiments.

The design of a torsion spring and the case studies that assist human motions using the proposed device will be presented at the conference.

References

[1] T. Hayashi, H. Kawamoto, and Y. Sankai, "Control method of robot suit HAL working as operator's muscle using biological and dynamical information," in *Proc. IEEE/RSJ Int. Conf. Intell. Robots Syst.: IROS 2005*, pp. 3063-3068.

[2] H. Kazerooni, J. Racine, L. Huang, and R. Steger, "On the control of the berkeley lower extremity exoskeleton (BLEEX)," in *Proc. IEEE Int. Conf. Robotics Autom.,: ICRA 2005*, pp. 4353-4360.

[3] A. Zoss, H. Kazerooni, and A. Chu, "Biomechanical design of the berkeley lower extremity exoskeleton (BLEEX)," *IEEE/ASME Trans. Mechatronics*, vol. 11, no. 2, pp. 128-138, 2006.

[4] K. Yamamoto, M. Ishii, H. Noborisaka, and K. Hyodo, "Stand alone wearable power assisting suit–sensing and control systems," in *Proc. IEEE Int. Workshop Robot Human Interactive Commun.: ROMAN 2004*, pp. 661-666.

[5] K. Kong and D. Jeon, "Design and control of an exoskeleton for the elderly and patients," *IEEE/ASME Trans. Mechatronics*, vol. 11, no. 4, pp. 428-432, 2006.

[6] J. Pratt, B. Krupp, and C. Morse, "Series elastic actuators for high fidelity force control," *Int. J. Ind. Robot*, vol. 29, no. 3, pp. 234-241, 2002.

[7] G. A. Pratt and Williamson M. W., "Series elastic actuators," in *Proc. IEEE/RSJ Int. Conf. Intell. Robotics Syst.: IROS 1995*, Pittsburgh, PA, pp. 399-406.

[8] D. W. Robinson, J. E. Pratt, D. J. Paluska, and G. A. Pratt, "Series elastic actuator development for a biomimetic walking robot," in *Proc. IEEE/ASME Int. Conf. Adv. Intell. Mech.: AIM 1999*, Atlanta, GA, pp. 561-568.

[9] K. Kong, J. Bae, and M. Tomizuka, "Control of rotary series elastic actuator for ideal force-mode actuation in human-robot interaction applications," *IEEE/ASME Trans. Mechatron*ics, vol. 14, pp. 105–118, 2009.

[10] Luminary Stellaris LM3S8962, *Luminary Micro, Texas Instruments*, [Online]. Available: http://www.luminarymicro.com/

[11] H. Lee and M. Tomizuka, "Robust motion controller design for high-accuracy positioning systems," *IEEE Trans. Ind. Electronics*, vol. 43, no. 1, pp. 48-55, 1996.